HHS Public Access

Author manuscript

Angew Chem Int Ed Engl. Author manuscript; available in PMC 2018 February 06.

Published in final edited form as:

Angew Chem Int Ed Engl. 2017 February 06; 56(7): 1815–1819. doi:10.1002/anie.201611195.

Elasticity in Macrophage Synthesized Biocrystals

Ms Elizabeth M. Horstman[a,‡], **Dr. Rahul K. Keswani**[b,‡], **Mr. Benjamin A. Frey**[c], **Mr. Phillip M. Rzeczycki**[b], **Mr. Vernon LaLone**[b], **Dr. Jeffery A. Bertke**[d], **Dr. Paul J. A. Kenis**[a], and **Dr. Gus R. Rosania**[b]

[a]Department of Chemical and Biomolecular Engineering University of Illinois, Urbana-Champaign 600 South Mathews Street, Urbana, IL 61801, USA

[b]Department of Pharmaceutical Sciences, College of Pharmacy University of Michigan, Ann Arbor 428 Church Street, Ann Arbor, MI 48109, USA

[c]Morgan State University, 1700 E Cold Spring Ln, Baltimore, MD 21251

[d]School of Chemical Sciences University of Illinois, Urbana-Champaign 505 South Mathews Street, Urbana, IL 61801, USA

Abstract

Supramolecular crystalline assembly constitutes a rational approach to bioengineer intracellular structures. Here, biocrystals of clofazimine (CFZ) that form in vivo within macrophages were measured to have marked curvature. Isolated crystals, however, showed reduced curvature suggesting that intracellular forces bend these drug crystals. Consistent with the ability of biocrystals to elastically deform, the inherent crystal structure of the principal molecular component of the biocrystals – the hydrochloride salt of CFZ (CFZ-HCl) – has a corrugated packing along the (001) face and weak dispersive bonding in multiple directions. These characteristics were previously found to be linked to the elasticity of other organic crystals. Internal stress in bent CFZ-HCl led to photoelastic effects on the azimuthal orientation of polarized light transmittance. We propose that elastic, intracellular crystals can serve as templates to construct functional microdevices with different applications.

Graphical abstract

Clofazimine Hydrochloride (CFZ-HCl) crystals, the primary component of CFZ-associated biocrystals that intracellularly crystallize in macrophage cells exhibit elastic behaviour. The multi directional interactions established via the salt-associated chloride (in HCl) and corrugated packing in the crystal structure of CFZ-HCl allow for the crystal's elasticity.

Correspondence to: Paul J. A. Kenis; Gus R. Rosania.

‡These authors contributed equally to this work.

Supporting information for this article is given via a link at the end of the document.

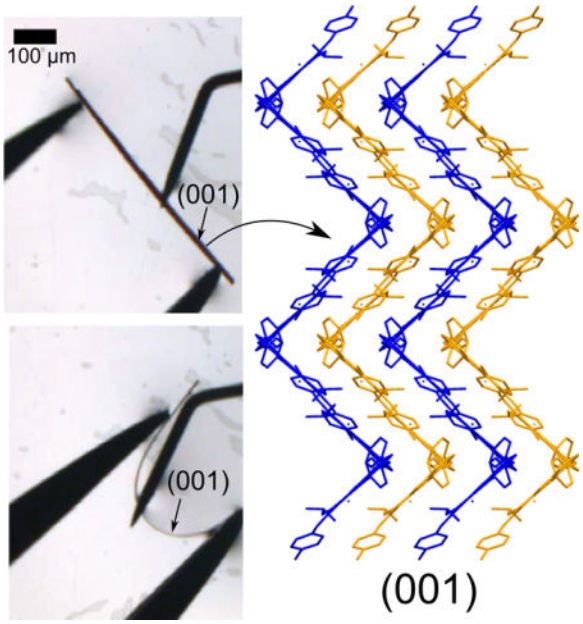

Keywords

crystal engineering; elasticity; biocrystals; clofazimine; X-ray diffraction

Abnormal morphology of crystals has been a subject of significant study over the last century[1–6]. Particularly, crystalline growth and distribution within living organisms such as cells, tissues and clinically in humans has allowed an understanding of how solid-state crystal chemistry can modulate biological and biophysical environments[7–12]. Specifically, the interaction of crystalline matter with cells such as macrophages within clinical microenvironments has garnered much attention[13–15]. Macrophages (Mφs) are critical self-nonself recognizing immune cells capable of maintaining mammalian homeostasis and resolving inflammatory conditions responsible for many diseases. Concurrently, Mφs are cellular “vacuum cleaners” eliminating foreign matter, typically referred to as xenobiotics. Such elimination may also be preceded by massive bioaccumulation, self-assembly and intracellular crystallization of sequestered foreign molecular agents such as clofazimine (CFZ), a red-pigmented, anti-inflammatory, antimycobacterial, FDA-approved drug molecule[16,17]. Specifically, CFZ accumulates within Mφs upon prolonged oral dosage in humans[18–21] and rodent models[13,22–24] (protocol in SI) to form biocrystals containing Clofazimine Hydrochloride (CFZ-HCl) crystalline domains[25].

In order to characterize the crystal structure and physical morphology of biocrystals, peritoneal and alveolar Mφs from an 8-week CFZ-fed mouse were harvested. Through brightfield microscopy, several cell-associated dark red crystals were identified, some of which were surprisingly curved (Figure 1a). Moreover, after 10 minutes, the crystals turned over likely due to mechanical forces exerted by its parent Mφ (Figure 1a). Upon closer inspection, we observed that another biocrystal in close proximity to the curved biocrystal also had a minor curvature that straightened out when the curved biocrystal flipped (Figure

1a). In light of this empirical evidence, we further characterized the biocrystals for their curvature (κ) within or isolated from Mφs (Figure 1b, S1). The curvature per unit length (κ/L) of biocrystals was significantly higher when present in peritoneal Mφs (4.8-fold change in mean, $p<0.005$) or alveolar Mφs (3.6-fold change in mean, $p<0.005$) compared to when isolated from Mφs. A greater number of biocrystals were found to be inherently straight or having zero curvature when isolated (26) than when present in peritoneal Mφs (10) or alveolar Mφs (18) (Figure 1b, S1). Such a reduction in curvature of isolated biocrystals are indicative of forces acting on the crystals curving them when present inside Mφs and secondly of inherent elasticity of the biocrystals.

Mechanical properties of crystals (moduli, plasticity, elasticity) are known to be dependent on the atoms, ions or molecules forming the crystals and the interactions between these particles (molecular packing and intramolecular bonding)[26–30]. Further, recent work has explored the relationship between elasticity in organic crystals and their molecular and structural properties. Ghosh and Reddy reported an elastic and bendable organic cocrystal solvate formed from caffeine, 4-chloro-3-nitrobenzoic acid and methanol with weak and dispersive C-H…π interactions in three nearly perpendicular directions, suggesting that elastic deformation is due to isotropic molecular packing[28,29]. Subsequently, Ghosh *et al.* studied n-benzylideneanilines and elucidated design rules for elastic organic crystals[26–28]. Accordingly, elastic organic crystals should have (1) multi-directional weak dispersive bonds that can be easily broken to dissipate energy as the crystal is bending and that can be easily formed when no force is applied and (2) corrugated packing along a crystallographic face to prevent long range dislocation within the crystal[26–28]. In these studies, when crystals did not align with these design rules, they did not demonstrate elastic behavior. As such, we explored if elasticity and curvature of biocrystals could be explained via these design parameters.

As the primary component of the biocrystals is CFZ-HCl, we hypothesized that the inherent crystal structure of CFZ-HCl plays a role in the flexibility (being able to adopt non-linear morphologies) and elasticity (being able to return to linear conformations upon removal of force) of the biocrystals. A synthetic crystallization route was developed to grow CFZ-HCl crystals with similar crystal structure to the biocrystals (protocol in SI). The synthetic CFZ-HCl crystals form dark red rectangular plates (Figure 2a) that closely resemble the crystal habit and color of the biocrystals (Figure 2b) as observed with brightfield microscopy. The CFZ-HCl crystals can grow to be much larger than the biocrystals allowing for optimal structural characterization. The p-XRD (Figure 2c) suggests a strong agreement in the observed peaks of CFZ-HCl with those from the biocrystals as previously reported[25]. Both samples show strong preferential orientation of the crystals along the (001) face, consistent with face indexing of single crystals (Figure S2). The most intense peak on the p-XRD spectra is the (002) peak due to a systematic absence at (00*l*) when $l=2n$ for Pbca space groups. Thus, the synthesized CFZ-HCl crystals are a suitable model for characterizing the mechanical behavior of the biocrystals.

Single crystal XRD was also performed to determine the crystal structure of CFZ-HCl. The CFZ-HCl crystals grow in an orthorhombic *Pbca* space group with unit cell parameters; $a=10.266$ Å, $b=19.828$ Å, and $c=24.156$ Å, $\alpha=\beta=\gamma=90°$ and $Z=8$ (CCDC number:

1497722). One CFZ and one HCl molecule make up the asymmetric unit (Figure 3a). Cl3 (the Cl associated with the HCl) associates with the CFZ through two N-H···Cl hydrogen bond interactions between N3-H···Cl3 and N4-H···Cl3 (D, d, θ: 3.172 Å, 2.376 Å, 166.45°, and 3.104 Å, 2.243 Å, 174.51°). The data set was solved to 99.8% completeness. Water was incorporated into the crystal structure at an occupancy of 0.13, and there was some disorder in the isopropyl group. The presence of water likely caused a change in the orientation of the isopropyl group, thereby contributing to the observed disorder (Figure S3). A summary of the unit cell parameters and diffraction data can be found in Table S1.

A key design feature of the CFZ-HCl crystal structure is the corrugated packing along the (001) face (Figure 3b,c). One CFZ-HCl molecule makes up one step of the zig-zag and together the steps make up one corrugated sheet. The steps of the zig-zag are held together with weak C-H···π and C-H···Cl interactions, highlighted by light blue dotted lines and orange solid lines respectively (Figure 3b). Cl3 is situated in the crease of the zig-zags and serves an anchor by coordinating with 3 additional molecules strengthening interactions within the crease and coordinating with adjacent sheets. Bond distances and angles are as follows: C14-H···Cl3, 3.503 Å, 2.724 Å, 139.72°, C24-H···Cl3, 3.457 Å, 2.757 Å, 131.19°, and C4-H···Cl3, 3.625 Å, 2.900 Å, 133.9°. These interactions are in 3 nearly perpendicular directions. Weak dispersive bonding between the sheets of the zig-zags from π···π interactions between the aromatic rings is also present (grey dotted lines, Figure 3b). Cl1 interacts with C5 (C5-H···Cl1, 3.516 Å, 2.937 Å, 120.48°) to create a ribbon of CFZ molecules down the b-axis (Figure S4). When viewed along the c-axis this interaction is located in the crease and it stabilizes interactions between the sheets of the zig zag. As such, the weak multi-directional interactions are located at critical parts of the zig-zag, particularly associated with Cl3 and support the previously proposed design rules for crystal elasticity[26]. The angle between the corrugated steps is ~82°. All intermolecular interactions are listed in Table S2. Face indexing of the crystal during XRD showed that the (001) face is the largest surface and which corresponds to the previous p-XRD data. The projection of the (001) face is shown in Figure 3c to better show the corrugated packing. Projections of all the crystallographic faces can be found in Figure S5.

Interestingly, while harvesting CFZ-HCl crystals for single crystals XRD, the crystals would noticeably bend when force was applied to pick up the crystals. As soon as the force was removed the crystals would promptly return to their original linear morphologies. Subsequently, video microscopy was performed of bending crystals with tweezers to further demonstrate their observed elastic response (Movie 1). Crystallization experiments yielded a very wide size distribution of crystals out of which crystals between 500 μm and 2 mm long and ~20 μm thick were chosen. The CFZ-HCl crystals typically lie with the (001) face normal to the substrate (Figure 4a). When a slight force was applied, the crystal rotated 90° about the a-axis (Figure 4b). When a force was applied to the (001) face, the crystal bent (Figure 4c–d) and assumed its original shape upon removal of the force (Figure 4e). The crystal arched again when a second force was applied, Figure 4f. As such, the crystals can be bent many times without noticeable deformation to the crystal. In one experiment a crystal was bent 8 times without noticeable deformation (Movie 2). However, upon applying a larger force, the crystal snapped and the crystalline fragments adopted the original straight configuration (Movies 1,2).

To confirm the elastic deformation of CFZ-HCl, polarization microscopy was performed as a way of measuring the photoelastic phenomena that is commonly observed with application of stress and development of strain[31]. In this particular study, linear dichroism could be measured using hardware configured on an epifluorescence-brightfield microscope[32,33] (See SI for protocol). Crystals were imaged under polarized light following which the anisotropy in transmittance and importantly, the azimuth (the polarization orientation that results in maximum transmittance) were computed (Figure 5)[34]. Crystals were first identified as regions with low transmittance (Figure 5ac). Given the structural packing of the CFZ-HCl lattice and absence of polycrystalline elements in the biocrystals, the azimuth distribution was expectedly isotropic across the crystal plane when unstressed and straight (Figure 5b). In contrast, the azimuth was anisotropic in the elastically deformed region of the crystal wherein two approximately orthogonal azimuthal orientations were measured (Figure 5d). In the concave region, the azimuth was perpendicular to the long axis of the crystal whereas in the convex region, the azimuth was retained along the long-axis of the crystal as observed in the straight crystals. Such anisotropy is clearly indicative of a stress network resulting in the development of an elastic strain through the crystal[35]. As such, given the extent of cross-interactions within the crystal lattice as described before (Figure 3, S2–S4), the development of an elastic stress-strain network through an expectedly isotropic crystal structure was accomplished and verified through photoelastic azimuth measurements.

Further, no differences in vibrational spectra (Raman) were evident before and after bending at the point of maximum curvature in these crystals (Figure S6). Naturally curved crystals also showed no differences in molecular vibrations compared to the reference CFZ-HCl crystals. Finally, the melting point for CFZ-HCl was measured to be 275°C (Figure S7), which is 53°C degrees higher than CFZ while other salts of CFZ also have melting points <246°C[36]. As indicated by their melting points, the salts of CFZ are more stable than CFZ. The stabilization of CFZ as CFZ-HCl within mammalian cells therefore favors the formation of a highly stable crystalline polymorph and as reported here has appropriate structural packing features, reinforced by the additional Cl from HCl (Cl3 in Figure 3a) that allow it to adapt to intracellular mechanical stressors.

In summary, we show that the inherent structural packing features of CFZ-HCl within biocrystals indeed contribute to their elasticity and naturally adjustable curvature. As such, formation of biocrystals mediated by Mφs leads to the development of elastic and curved crystalline elements with structural packing features that showcase the classical design rules designated for organic crystal flexibility[26–29]. The presence of CFZ biocrystals in the Mφ endows them with potent anti-inflammatory characteristics[37,38] and specific fluorescent[39] and photoacoustic[40,41] signatures for cellular optical tracking. Such dual therapeutic and diagnostic (theranostic) applications make biocrystals a potent cellular device that could be harnessed for biomedical applications. Mφ-mediated crystallization is an important example of how these cells self-assemble a crystal with features that allow for easier adaptability to the mechanical environment of the cell, thereby allowing a massive drug loading within the cell. Importantly, the additional Cl (in HCl) is most likely reinforced within CFZ biocrystals through the presence of multiple chloride channels in macrophages and their highly regulated role in cellular physiology[42–44]. Here, we show that the salt chloride also plays

an integral role in the structural stability and intracellular mechanical adaptation via elasticity.

Furthermore, mechanical flexibility of exogenous elements within cells could be a critical design parameter toward engineering organic intracellular constructs to endow cells with unnatural yet stable and beneficial features for therapeutic applications. Finally, viscoelasticity, pressures and connected mechano-transductive elements are innately connected to inflammatory cell phenotypes[45–49]. As such, the mechanochemical characterization of intracellular properties could be important for cell-based mechano-biological applications leading to a new class of pharmaceutics: mechano-pharmaceutics.

Supplementary Material

Refer to Web version on PubMed Central for supplementary material.

Acknowledgments

We would like to thank the National Science Foundation (NSF) for a Graduate Research Fellowship to EMH (DGE-1144245), National Institute of General Medical Sciences (NIGMS) for funding support to GRR (R01GM078200), University of Michigan of Office of Research MCubed Program funding to GRR, Michigan Institute for Clinical & Health Research Pilot Seed funding to GRR and RKK (NIH: UL1TR000433) and the Interdisciplinary REU (Research Experiences for Undergraduates) Program housed in the College of Pharmacy, University of Michigan for funding BAF through the NSF-Division of Biological Infrastructure (NSF-DBI) (DBI-1263079). We acknowledge the support of Dr. Gislaine Kuminek, Dr. Nair Rodriguez-Hornedo, Dr. Gi Sang Yoon and Sudha Sud, Department of Pharmaceutical Sciences, College of Pharmacy, University of Michigan for help with DSC and animal experiments; Dr. Danielle Gray, George L. Clark X-ray Facility and 3M Materials Laboratory, University of Illinois for discussion about crystallographic data, and Lucas C. Gonzalez, Department of Chemical and Biomolecular Engineering, University of Illinois for help with crystallization experiments.

References

1. Spencer LJ. Mineral Mag. 1921; 19:263–274.
2. Panda MK, Ghosh S, Yasuda N, Moriwaki T, Mukherjee GD, Reddy CM, Naumov P. Nat Chem. 2015; 7:65–72. [PubMed: 25515892]
3. Reddy CM, Gundakaram RC, Basavoju S, Kirchner MT, Padmanabhan KA, Desiraju GR. Chem Commun (Camb). 2005; 1:3945–7.
4. Koshima H, Matsuo R, Matsudomi M, Uemura Y, Shiro M. Cryst Growth Des. 2013; 13:4330–4337.
5. Godwod K, Nagy AT, Rek Z. Phys Status Solidi. 1976; 34:705.
6. Terao F, Morimoto M, Irie M. Angew Chemie – Int Ed. 2012; 51:901–904.
7. Baumgartner J, Morin G, Menguy N, Perez Gonzalez T, Widdrat M, Cosmidis J, Faivre D. Proc Natl Acad Sci. 2013; 110:14883–14888. [PubMed: 23980143]
8. Siponen MI, Legrand P, Widdrat M, Jones SR, Zhang WJ, Chang MCY, Faivre D, Arnoux P, Pignol D. Nature. 2013; 502:681–684. [PubMed: 24097349]
9. Wang Y, Lomakin A, Hideshima T, Laubach JP, Ogun O, Richardson PG, Munshi NC, Anderson KC, Benedek GB. Proc Natl Acad Sci. 2012; 109:13359–13361. [PubMed: 22847421]
10. Weller PF, Goetzl EJ, Austen KF. Proc Natl Acad Sci U S A. 1980; 77:7440–7443. [PubMed: 6261258]
11. Mulay SR, Anders HJ. N Engl J Med. 2016; 374:2465–2476. [PubMed: 27332905]
12. Sullivan DJ Jr, Gluzman IY, Goldbery DE. Science. 1996; 271:219–222. [PubMed: 8539625]
13. Aplin RT, McDougall AC. Experientia. 1975; 31:468–469. [PubMed: 1120525]
14. Vicari P, Sthel VM. N Engl J Med. 2015; 373:e27. [PubMed: 26630152]

15. Martinon F, Pétrilli V, Mayor A, Tardivel A, Tschopp J. Nature. 2006; 440:237–41. [PubMed: 16407889]
16. Cholo MC, Steel HC, Fourie PB, Germishuizen WA, Anderson R. J Antimicrob Chemother. 2012; 67:290–8. [PubMed: 22020137]
17. Barry VC, Belton JG, Conalty ML, Denneny JM, Edward DW, O'Sullivan JF, Twomey D, Winder F. Nature. 1957; 179:1013–1015. [PubMed: 13430770]
18. Levy L. Am J Trop Med Hyg. 1974; 23:1097–1109. [PubMed: 4611255]
19. Belaube P, Devaux J, Pizzi M, Boutboul R, Privat Y. Int J Lepr Other Mycobact Dis. 1983; 51:328–330. [PubMed: 6685693]
20. Banerjee DK, Ellard GA, Gammon PT, Waters MFR. Am J Trop Med Hyg. 1974; 23:1110–1115. [PubMed: 4429180]
21. McDougall AC, Horsfall WR, Hede JE, Chaplin AJ. Br J Dermatol. 1980; 102:227–230. [PubMed: 7387877]
22. Baik J, Stringer KA, Mane G, Rosania GR. Antimicrob Agents Chemother. 2013; 57:1218–30. [PubMed: 23263006]
23. Baik J, Rosania GR. PLoS One. 2012; 7:e47494. [PubMed: 23071814]
24. Conalty ML, Jackson RD. Br J Exp Pathol. 1962; 43:650–654.
25. Keswani RK, Baik J, Yeomans L, Hitzman C, Johnson A, Pawate A, Kenis PJA, Rodríguez-Hornedo N, Stringer KA, Rosania GR. Mol Pharm. 2015; 12:2528–2536. [PubMed: 25926092]
26. Ghosh S, Mishra MK, Kadambi SB, Ramamurty U, Desiraju GR. Angew Chemie Int Ed. 2015; 54:2674–2678.
27. Ghosh S, Mishra MK, Ganguly S, Desiraju GR. J Am Chem Soc. 2015; 137:9912–9921. [PubMed: 26192986]
28. Ghosh S, Reddy CM. Angew Chemie – Int Ed. 2012; 51:10319–10323.
29. Chen CT, Ghosh S, Reddy CM, Buehler MJ. Phys Chem Chem Phys. 2014; 16:13165–71. [PubMed: 24865365]
30. Hayashi S, Koizumi T. Angew Chemie – Int Ed. 2016; 55:2701–2704.
31. Mueller H. Phys Rev. 1935; 47:947–957.
32. Min KA, Rajeswaran WG, Oldenbourg R, Harris G, Keswani RK, Chiang M, Rzeczycki P, Talattof A, Hafeezma M, Horobin R, et al. Adv Sci. 2015; 2:1500025.
33. Koike-Tani M, Tani T, Mehta SB, Verma A, Oldenbourg R. Mol Reprod Dev. 2015; 82:548–562. [PubMed: 23901032]
34. Mehta SB, Shribak M, Oldenbourg R. J Opt. 2013; 15:94007.
35. Curtis A, Sokolikova-Csaderova L, Aitchison G. Biophys J. 2007; 92:2255–61. [PubMed: 17189310]
36. Bolla G, Nangia A. Cryst Growth Des. 2012; 12:6250–6259.
37. Yoon GS, Sud S, Keswani RK, Standiford TJ, Stringer KA, Rosania GR. Mol Pharm. 2015; 12:2517–2527. [PubMed: 25909959]
38. Yoon GS, Keswani RK, Sud S, Rzeczycki P, Murashov M, Koehn T, Standiford TJ, Stringer KA, Rosania GR. Antimicrob Agents Chemother. 2016; 60:3470–3479. [PubMed: 27021320]
39. Keswani RK, Yoon GS, Sud S, Stringer KA, Rosania GR. Cytom Part A. 2015; 87A:855–867.
40. Tian C, Keswani RK, Gandikota G, Rosania GR, Wang X. Proc SPIE. 2016; 9708:97084L–1.
41. Keswani RK, Tian C, Peryea T, Girish G, Wang X, Rosania GR. Sci Rep. 2016; 6:23528. [PubMed: 27000434]
42. Jentsch TJ. J Physiol. 2007; 578:633–40. [PubMed: 17110406]
43. Graves AR, Curran PK, Smith CL, Mindell JA. Nature. 2008; 453:788–92. [PubMed: 18449189]
44. Jiang L, Salao K, Li H, Rybicka JM, Yates RM, Luo XW, Shi XX, Kuffner T, Tsai VWW, Husaini Y, et al. J Cell Sci. 2012; 125:5479–88. [PubMed: 22956539]
45. Patel NR, Bole M, Chen C, Hardin CC, Kho AT, Mih J, Deng L, Butler J, Tschumperlin D, Fredberg JJ, et al. PLoS One. 2012; 7:e41024. [PubMed: 23028423]
46. Adlerz KM, Aranda-Espinoza H, Hayenga HN. Eur Biophys J. 2016; 45:301–309. [PubMed: 26613613]

47. Pugin J, Dunn I, Jolliet P, Tassaux D, Magnenat JL, Nicod LP, Chevrolet JC. Am J Physiol. 1998; 275:L1040–50. [PubMed: 9843840]
48. Shiratsuchi H, Basson MD. Am J Physiol Cell Physiol. 2004; 286:C1358–66. [PubMed: 14761895]
49. Shin HY, Frechette DM, Rohner N, Zhang X, Puleo DA, Bjursten LM. J Tissue Eng Regen Med. 2013; 2:408–417.

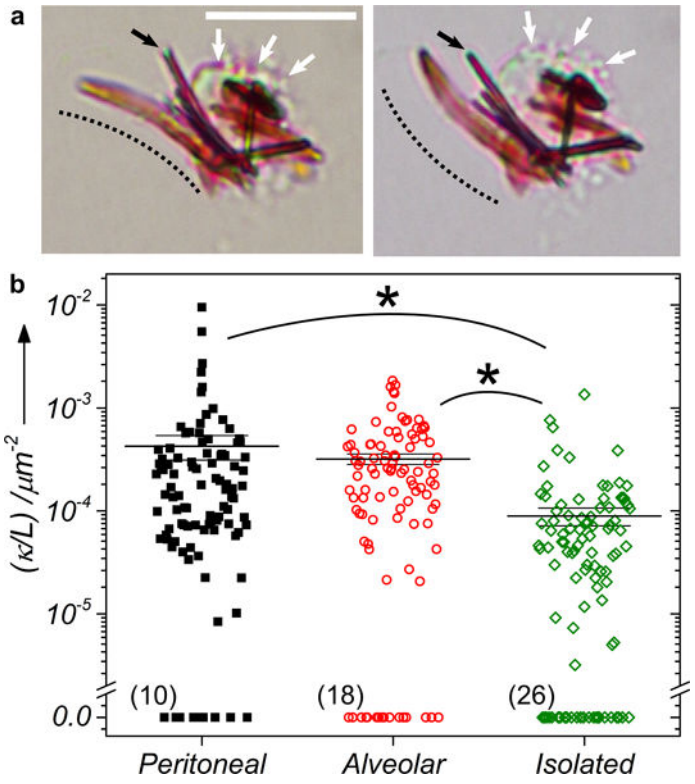

Figure 1.

a) Peritoneal macrophages from a CFZ-fed mouse with the curvature of the curved biocrystal marked with dotted lines (white arrows show cell membrane, black arrows mark the crystal in physical contact with the first curved crystal). Scale bar – 10 μm. b) Curvature per unit arc length (κ/L) of biocrystals in peritoneal Mφs or alveolar Mφs or when isolated from splenic Mφs. (n=100 biocrystals, * – $p<0.005$. The wider and thick horizontal line indicates the mean of the distribution whereas the other smaller two lines indicate the mean ± SE. Number in brackets indicates the number of biocrystals measured to have zero curvature.

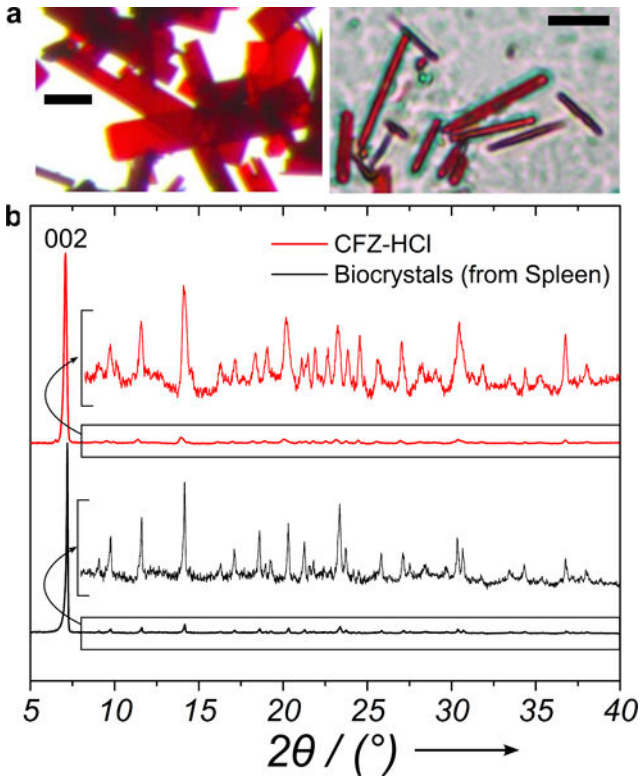

Figure 2.

Optical micrograph of a) synthesized CFZ-HCl crystals, Scale bar=50 μm and b) harvested biocrystals from a 8-week CFZ-fed mouse spleen, Scale bar=10 μm. c) Powder X-ray diffraction data from biocrystals and CFZ-HCl crystals. Both samples display preferential orientation favoring the (001) face. The diffraction data from 2θ=8–40° is zoomed in for convenient comparisons.

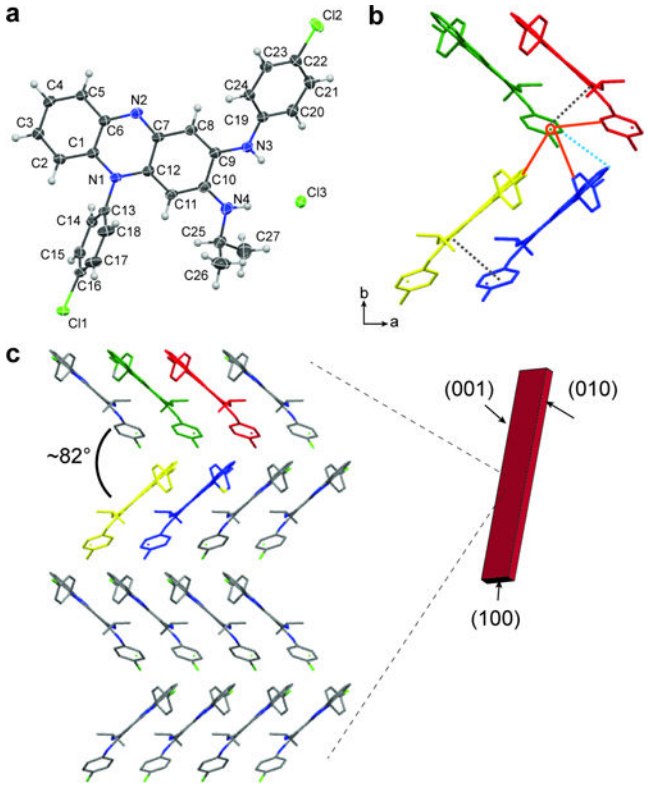

Figure 3.

a) Asymmetric unit of CFZ-HCl displayed as an ellipsoid plot with 50% probability. The atomic positions for all non-hydogen atoms are labeled. b) One section of the corrugated packing with solid orange lines indicating CH…Cl interactions, C-H…π indicated with a light blue dotted line and π…π interactions indicated by light grey dotted lines (unit cell looking along the caxis). The molecules are displayed as capped sticks with the hydogen atoms removed for better visualization of the crytals packing. c) Crystallographic projections of packing along the (001) face showing the corrugated packing. The projection is made up of 2 × 2 × 0.5 (a × b × c) unit cells.

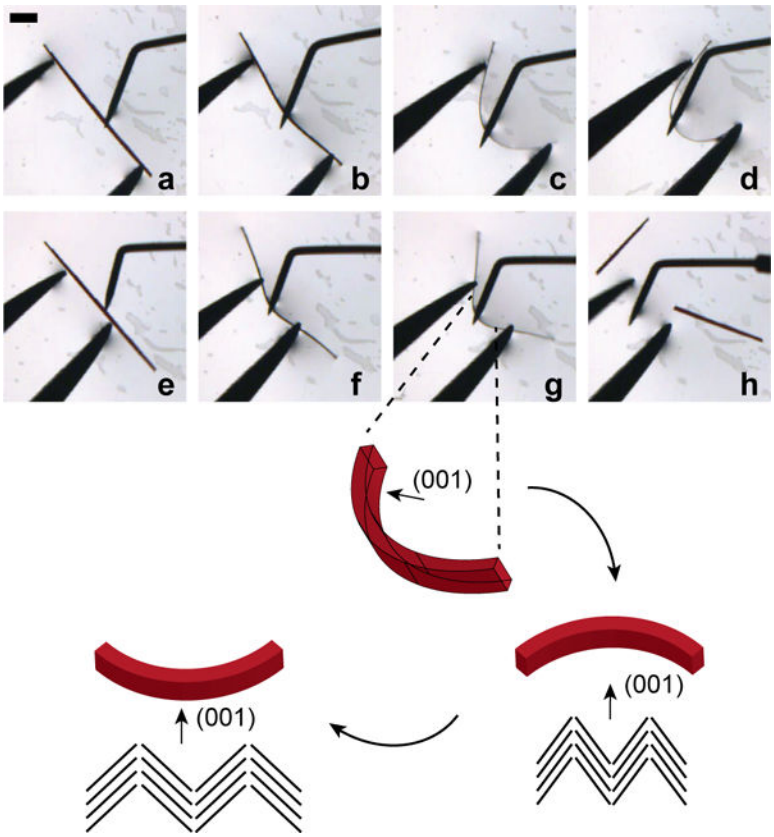

Figure 4.

a–d) A CFZ-HCl crystal was bent by applying a force with a crystallization probe while the crystal was held stationary against a pair of tweezers. e) The force was removed and the crystal quickly regained the original position before f) another force was applied to the crystal. Scale bar is 100 um. The bottom schematic shows how the angle of corrugation would look like on the convex and concave edges of the crystal during bending.

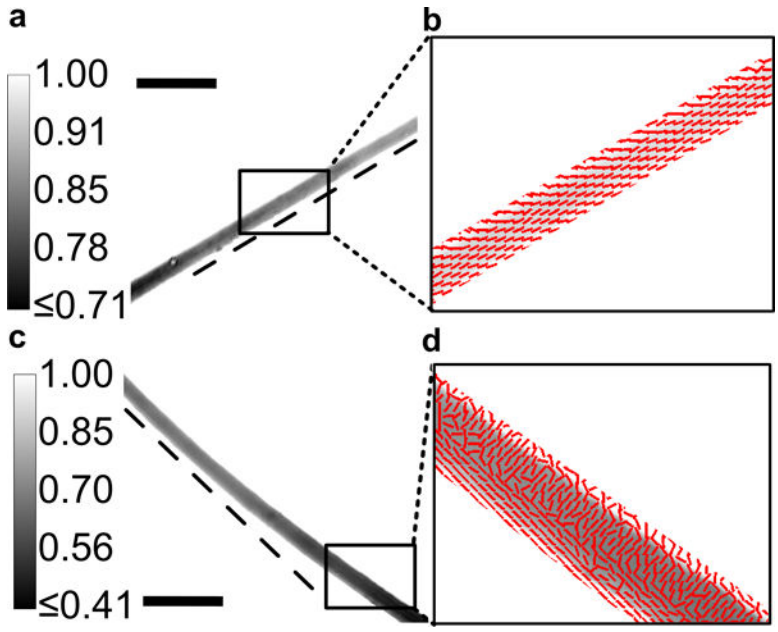

Figure 5.

a) Computed transmittance Image of a a–b) straight vs c–d) bent crystal. Calibration bar in (a,c) shows the range of transmittance. Dark regions (with low transmittance) follow the crystal with the dotted tangential line from one edge of the crystal confirming the curvature in the crystal. Azimuth – polarization orientation of maximum transmittance overlayed on the transmittance image indicating unidirectional axes in the b) straight crystal while in the d) bent crystal, there is a bidirectional axes depending on the direction of compressional (inward bending edge leads to an orthogonal axes) or tensile stress (outward bending edge leading to a longitudinal axis). Scale bar in a,b = 100 μm.